

Received 20 January 2025, accepted 4 February 2025, date of publication 13 February 2025, date of current version 21 February 2025.

Digital Object Identifier 10.1109/ACCESS.2025.3541870

RESEARCH ARTICLE

A Silicon Photonic 32-Input Coherent Combiner for Turbulence Mitigation in Free Space Optics Links

LORENZO DE MARINIS¹, (Member, IEEE),
PETER SEIGO KINCAID¹, (Member, IEEE), YANN LUCAS²,
LEA KRAFFT², VINCENT MICHAU², MATTEO CHERCHI^{3,4},
MIKKO KARPPINEN³, AND GIAMPIERO CONTESTABILE¹

¹Scuola Superiore Sant'Anna, 56124 Pisa, Italy

²DOTA, ONERA, Université de Paris-Saclay 92320 Châtillon, France

³VTT Technical Research Centre of Finland, 02044 Espoo, Finland

⁴Xanadu Quantum Technologies Inc., Toronto, ON M5G 2C8, Canada

Corresponding author: Lorenzo De Marinis (lorenzo.demarinis@santannapisa.it)

This work was supported in part by the European Union (EU) Horizon 2020 Programme through the Actphast 4R Project under Grant 779472; and in part by Valtion Teknillinen Tutkimuskeskus (VTT's) Si photonics activities are part of the Research Council of Finland Flagship Programme, Photonics Research and Innovation (PREIN) under Grant 346545.

ABSTRACT Free space optical links promise high data rates for future wireless communications systems, but performance is degraded by turbulence, limiting the potential use cases. A photonic integrated circuit (PIC) for turbulence mitigation is reported and characterized, which coherently combines 32 input optical signals into a single output fiber. The PIC was fabricated using a low-loss, and high integration density, thick silicon-on-insulator (SOI) process and packaged with 32 input fibers and 1 output fiber. The basic building block is a 2×2 Mach-Zehnder interferometer (MZI) with an external (to the MZI branches) and an internal thermal phase shifter, and a bandwidth in excess of 80 kHz. The PIC monolithically integrates 31 MZIs and 31 germanium photodetectors and is suitable in principle for turbulence mitigation in LEO-ground and horizontal free space optics links. Improvements to the device for the coherent combination of 64 inputs and for the reduction of insertion losses are also discussed.

INDEX TERMS Adaptive optics, coherent combiner, free space optics, silicon photonics, turbulence mitigation.

I. INTRODUCTION

Free space optical communications (FSO) have been the subject of active development for several decades. FSO links offer the potential for data rates currently inaccessible with radio frequencies, with experimental systems able to sustain terabits/s data rates over km distances [1]. Generally speaking, in all situations where laying optical fibers is either too expensive or not feasible, FSO can provide a viable solution [2], and is expected to play a crucial role as one of the technologies enabling 5G/6G [3] and satellite communications [4], including quantum links [5]. Furthermore,

the short wavelength allows beams of high directivity which therefore limits possible interference problems and reduces the power required for transmission. The choice of the fiber optics C-band and the coupling of the free space beam to a single mode fiber (SMF) allow the use of existing fiber optic communication technologies and systems, thereby limiting deployment costs. However, the propagation of the beam through turbulent atmosphere is detrimental to the SMF coupling efficiency. Adaptive optics is envisaged for turbulence mitigation in future optical ground stations dedicated to ground-satellite links (GEO or LEO) to maximize the detected signal allowing throughputs of 10 to 100 Gbps per channel [6], [7], [8], [9], some demonstrations of horizontal optical links have also been

The associate editor coordinating the review of this manuscript and approving it for publication was Liam Barry.

carried out [10], [11], with a transmission capacity exceeding 1 Tbps [12].

Classic adaptive optics methods for turbulence mitigation require a deformable mirror and a wavefront sensor, with relatively large footprint. Furthermore, wavefront sensors are well suited to astronomical observation and to optical links close to the zenith, but are sensitive to the strong scintillation encountered when the beams propagate in the lower atmosphere over distances greater than a few kilometers [13]. An alternative solution based on modal decomposition and subsequent guided wave coherent combination was proposed for SMF coupling [14]; Fig. 1 illustrates the principle in the case of a satellite to ground FSO link with beam propagation through a turbulent atmosphere. Here, the distorted field is first decomposed into N guided waves via a spatial demultiplexer, which are then added coherently within a photonic circuit whose phase shifters correct the fluctuations in the complex amplitudes of the guided waves in real time. In this scheme, the phase shifters are controlled in a closed-loop, with the correction to be applied estimated from the output signals by adding a rapid, low amplitude modulation to the phase shifter control signals [15], [16], [17]. Finally, the constructively recombined output of the photonic circuit is coupled to an output SMF. Performing the coherent combination with bulk fiber components is impractical because of large size, the requirement of matched optical paths and for mechanical stability issues. For these reasons, the use of Photonic Integrated Circuits (PIC) was proposed [14], which offer small footprint, mechanical and thermal stability, and low mismatch between optical paths [18], [19], [20]. This solution allows to overcome both the disadvantages of the large footprint and the susceptibility to strong scintillation associated with classic adaptive optics assemblies. An example of a photonic circuit architecture for the coherent addition of guided waves is presented in Fig. 2.

The practical specifications of coherent combiners may be deduced as a first approximation from that of the equivalent classic adaptive optics system. The performance depends firstly on the number of spatial modes, i.e., the number of actuators in the deformable mirror or the number of guided waves in the spatial multiplexer. The closed-loop correction frequency also plays an important role for both devices; when using a PIC, aside from the correction signal, an additional low amplitude tone must be applied to the phase shifters, with its relative frequency as high as possible to avoid any interference with the control signal. According to N. Védrenne [21], a few dozen actuators would be required for AO dedicated to LEO-ground links, with the number increasing to 100-200 for GEO-ground links; a correction frequency of between 2 and 10 kHz would be required for LEO-ground links due to the movement of the satellite, this is 10 times lower for GEO-ground links. Finally, the main interest of the correction lies in the increase in power of the collected signal, hence the losses in the component must be minimized. For comparison, the typical optical losses of

classic adaptive optics systems are of the order of 5 dB, due to the presence of a few dozen optical surfaces in the beam path and SMF coupling.

In the literature, previous coherent combination schemes were demonstrated with up to 16 inputs on a single PIC fabricated with SOI [18], [19], [20], and up to 32 effective inputs by combining four 8 input PICs [22]. Recently, the fabrication of a 45 input PIC for turbulence mitigation was reported, but without integrating the photodetectors [23]. In this paper, we extend our previous work [24], reporting the design, fabrication, and characterization of an integrated coherent combiner suitable for 32 inputs/modes. As the scalability and footprint of the device is governed by losses and integration density, we fabricated the PIC using the low-loss silicon thick SOI platform available at VTT Finland [25]. The 32 input configuration with phase shifter bandwidth in excess of 50 kHz, is suitable in principle for correcting the effects of atmospheric turbulence on any LEO-ground link. Indeed, these parameters are close to those of the AOptix R3.1 classic adaptive optics element used as part of the ORCA (Optical RF Communications Adjunct) [26]. The fabricated chip demonstrated a bandwidth larger than 80 kHz, with phase shifters able to provide more than 6π of phase shift correction. The integrated germanium photodetectors exhibited a responsivity of 0.8 A/W, a dark current < 2 nA, and a bandwidth > 2 GHz with zero bias applied. The remainder of the paper is organized as follows. First, we discuss the features of photonic integration platforms and outline their shortcomings for the development of coherent combiners. We then report the design, fabrication and packaging of the coherent combiner. In the device characterization section, we report the main characterization measurements of the PIC and its building blocks: phase shifters, Mach-Zehnder interferometers, photodetectors, and I/O losses. This is followed by a discussion section on our findings and prospected devices based on the same technology, exploring their applications in realistic FSO link. Finally, we summarise the work in the conclusions.

II. COHERENT COMBINER FOR FREE SPACE OPTICS

There are several photonic integration platforms suitable for the manufacturing of coherent combiners. Each one with its own characteristics, strengths, and limitations. However, the need of scaling the structure towards a high number of inputs poses a stringent requirement in terms of compactness: the larger the number of inputs, the larger the number of combining elements (MZIs) to be integrated and thus the associated device footprint. This renders a fabrication with the Indium Phosphide technology unpractical, due to the large bending radius and typical attainable yields [27]. The emerging lithium niobate on insulator technology (LNOI) platform provides very low losses and medium-short bending radius (≤ 100 μm). However, its lack of maturity poses limits to practical usage: just one company in the world currently offers wafer-scale fabrication, furthermore LNOI phase

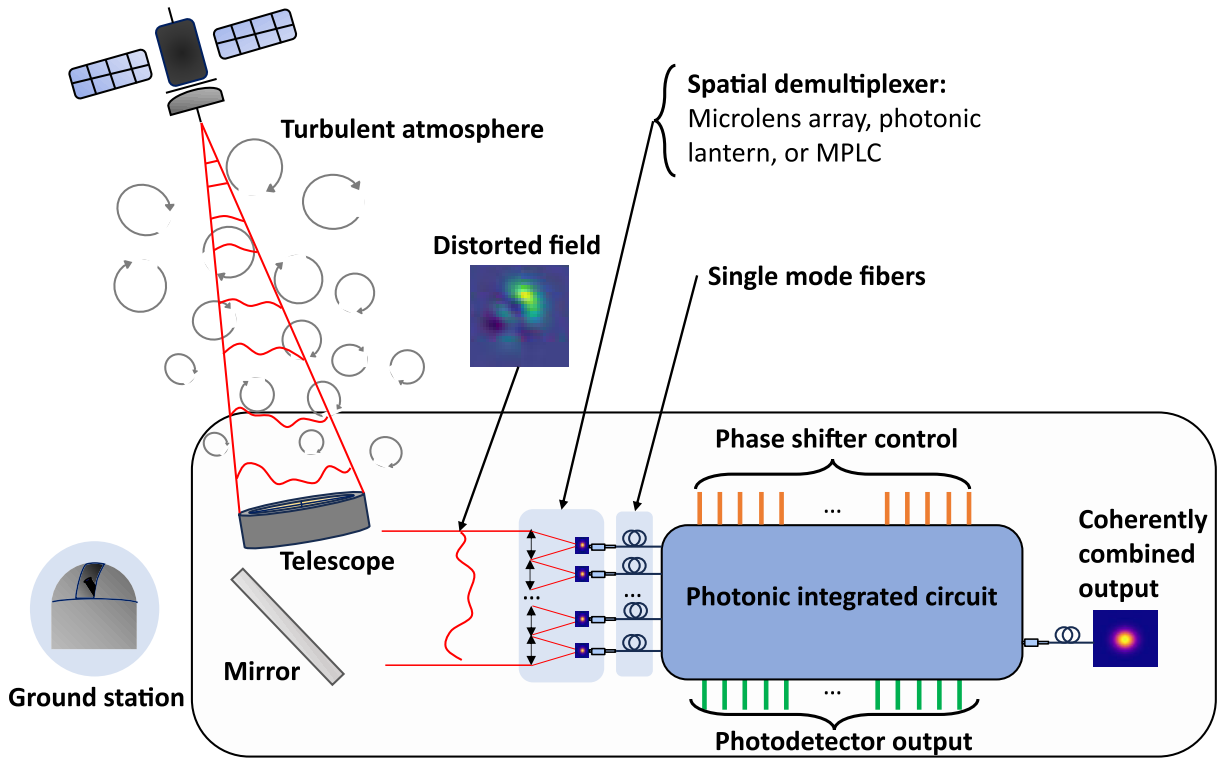


FIGURE 1. Satellite-to-ground FSO communication with distorted fields, modal decomposition followed by PIC coherent combination after FSO beam reception by the ground station telescope.

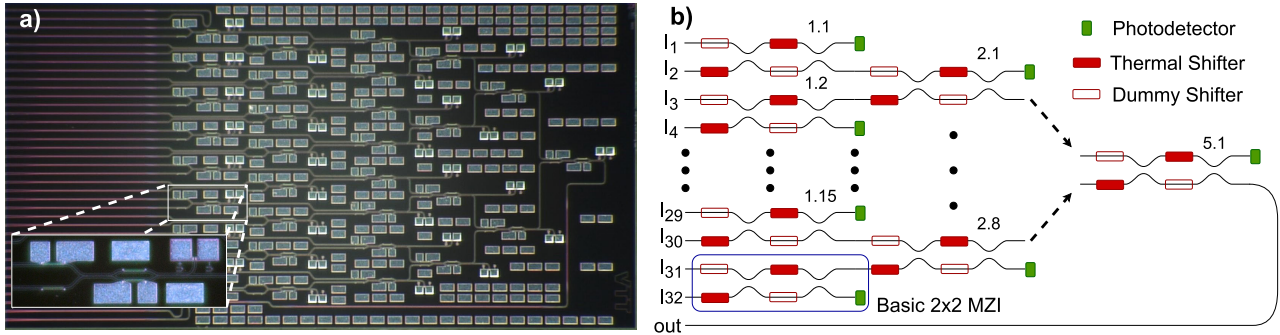


FIGURE 2. a) Photo of the as-fabricated Thick SOI chip with a magnification of the basic MZI; b) scheme of the coherent combiner architecture.

shifters notoriously suffer from DC drifts, it lacks integrated PDs, and the optical I/O with fiber arrays has low yield and high losses. The Silicon Nitride platform offers a more robust process, with low coupling and propagation losses, and the possibility to hybridly integrate photodetectors. However, the scaling of structures in silicon nitride is hindered by the high bending radius of the waveguides, and the large power consumption (and related thermal crosstalk) of the thermal phase controllers.

Conversely, silicon photonics meets all the requirements as it offers compact structures (μm bends) and integrated detectors, while providing high yields with a robust process which inherited the maturity of the CMOS technology [28]. Among the various silicon platforms, the thick SOI process

available at VTT was ideal for fabricating the coherent combiner demonstrator. This fabrication platform is based on $3\ \mu\text{m}$ thick waveguides where the optical field modes are almost completely confined in the silicon core. This gives small propagation losses ($\sim 0.1\ \text{dB/cm}$ in the C-band), low polarization dependency, and dense integration thanks to Euler bends that can provide an effective bending radius as small as $1.3\ \mu\text{m}$ [25]. Optical I/O is facilitated by the horizontal taperings of waveguides on chip, from $3\ \mu\text{m}$ to $12\ \mu\text{m}$. The tapers work as spot-size converters to improve the coupling to SMFs. In addition, VTT offers an SOI optical waveguide interposer chip as a vertical spot-size converter to further increase the coupling efficiency between fiber arrays and the SOI PIC [25]. Using the optical

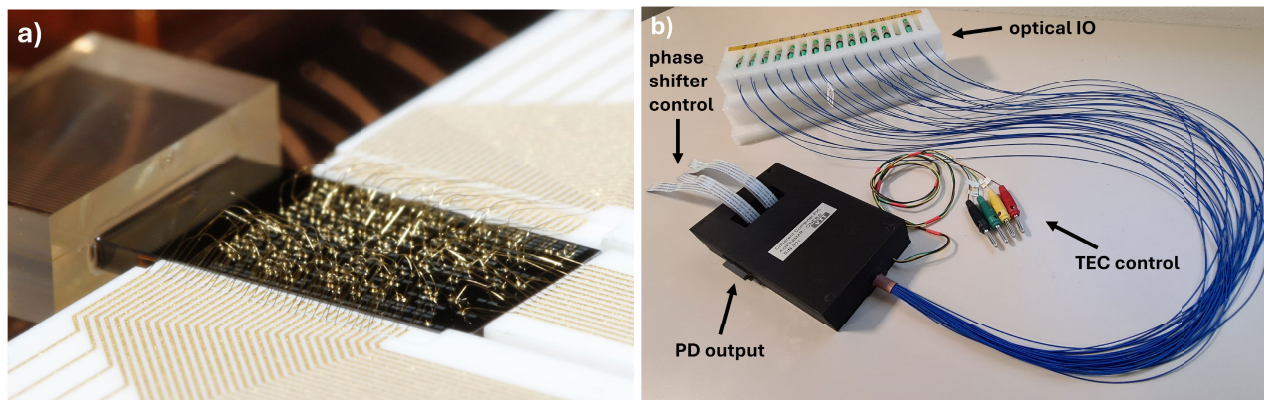


FIGURE 3. a) Photo of the PIC undergoing packaging after wire bonding to an electrical interposer and fixing the optical IO to a fiber array; b) Finished package with optical IO coupled to SMF fibers, thermo-electric control (coloured cables) and DC IO ports for thermal shifter control and photodiode output.

interposer, approximately 1.5-2 dB I/O coupling losses are possible, depending on the detailed structure of the I/O facet. Moreover, the available integrated germanium photodiodes have a low dark current and a responsivity of ≈ 0.8 A/W.

When scaling structures that rely on thermo-optic phase shifters, assuring a high thermal isolation is of paramount importance for correct functionality. However, high integration density with close structures often leads to poor thermal isolation with an evident footprint-isolation trade-off to be made. Nonetheless, the VTT process tackles this issue: the thermal phase shifters are made of doped silicon implanted close to the optical waveguides for high efficiency, with isolation trenches that prevent thermal cross-talk between close structures. The heaters have a power consumption associated with a π shift in phase (P_π) lower than 40 mW, and a bandwidth of several tens of kHz, making them suitable for the turbulence mitigation application. Moreover, the heaters allow for several π of phase shift (on the order of 5-6 π before failure), a feature needed to reduce the fading induced by an abrupt 2π phase shift from the adaptive optics correction algorithm, which occurs when the upper limit in phase shift is reached.

Leveraging the features of the thick-SOI process, we were able to design an integrated coherent combiner with 32-inputs. The combination is performed with a binary tree architecture, where 2×2 MZIs are used to coherently combine lightwave pairs [29]. Fig. 2a reports a photo of the naked fabricated PIC, with the enclosed close up displaying the basic 2×2 MZI element. The MZI structure consists of two inputs, one of which has a thermal phase shifter (the “external” shifter), a 2×2.3 -dB multimode interferometer (MMI) which splits evenly to two internal branches, one with another phase shifter (the “internal” shifter). Another MMI follows with one output coupled to a monitor photodiode (PD), and the other which feeds into the next MZI or, in the case of the last MZI, to the output port. The external phase shifter sets the correct relative phase between the two incoming lightwaves such that the power in both internal

branches is equal, the internal phase shifter then directs all optical power to the correct exit. The power at the exit of each MZI may be optimised using a routine which minimises the power at the monitor PDs by opportune control of the two phase shifters. The MMI should be well balanced for a MZI to be able to combine channels with different phase and amplitude. Furthermore, optical cross talk needs to be minimal for the modulation based control algorithm not to fail. Fig. 2b shows the equivalent schematic of the whole structure, highlighting the basic 2×2 MZIs with a blue rectangle; to ensure maximally balanced paths within the MZIs, some non-connected, or “dummy”, phase shifters were placed. The MZIs are numbered in an ascending fashion following columns and rows, e.g., MZI 1.15 is the 15th from the top of the PIC in the first column and MZI 3.1 is the topmost of the third column. 32 polarization maintaining single mode fibers (SMFs) are edge-coupled to the side of the chip to provide the optical I/O, the inputs feed into the first row of MZIs (1.1-1.16). The optical connections within (and between) the MZIs are strip waveguides with a height of $3 \mu\text{m}$ and a width of $1.875 \mu\text{m}$, which ensure high mode confinement and small bending radius, but in which higher order modes are supported. To remove any optical power coupled to higher order modes, input lightwaves pass through a 2 mm long section of straight rib waveguides, before coupling to the MZIs. This section can be made significantly shorter, but has been kept as long as possible considering the footprint of our chip with minimal optical losses associated with the thick SOI waveguides. The silicon chip contains a total of 31 MZIs, 62 thermal shifters, and 31 PDs, within a footprint of $10 \times 5 \text{ mm}^2$.

The chip was packaged by VTT, the electrical pads were wire bonded to a ceramic electrical interposer, and then to a PCB, and it was enclosed with a thermoelectric cooler (TEC) element in an aluminium case to allow thermal dissipation. For technical issues, it was not possible to include the optical interposer in the packaged prototype device. This was because of small positioning error of the lane etching

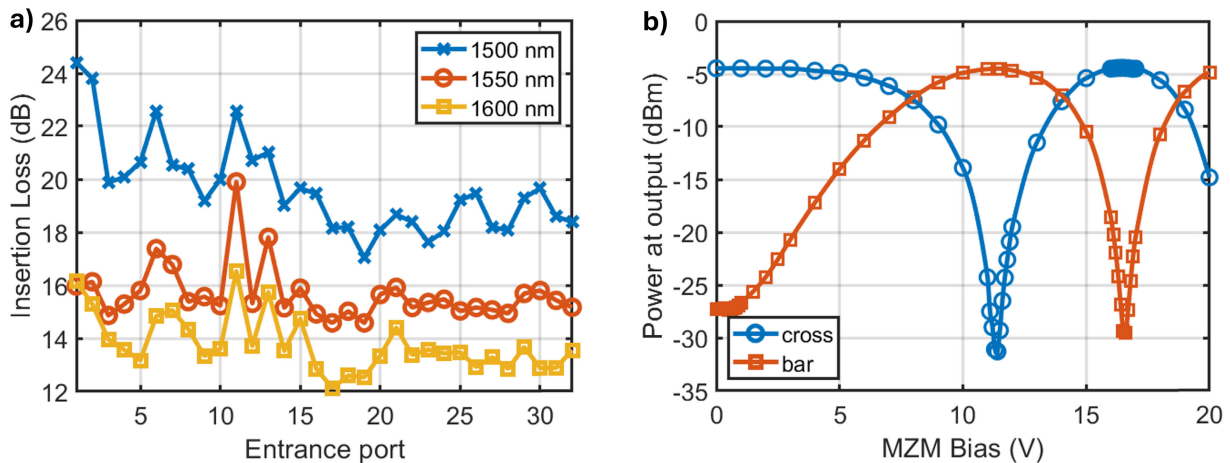


FIGURE 4. a) Total insertion loss at optical output as a function of input port and wavelength. b) Measured interference of MZI 1.1 for bar and cross port when the external laser is coupled at inputs 2 and 1 respectively.

step which defines the optical I/O facet of the PIC. This error prevented the attachment of the interposer chip close enough to the waveguide facet for efficient optical coupling. For this reason, the fiber array was directly interfaced to the PIC spot size converters, with a negative impact on the coupling losses as discussed in the following section. Fig. 3a shows the chip after wirebonding and attachment of the optical fiber array, Fig. 3b shows the fully-packaged chip. The coloured DC cable connections are for piloting the TEC, on the case the laterally placed DC connectors are for the monitor photodiodes, and the central DC connectors are for MZI control.

III. DEVICE CHARACTERIZATION

The packaged chip was characterised with an external cavity tunable laser, individually coupled to the optical inputs. The MZIs were driven with a custom digital to analog converter (DAC), whose output ranges between 0 and 32 V. The output port was connected to a PD for analysis. The temperature of the TEC was set to 20 °C unless otherwise specified. Information about the measurement instrument models, complementary figures and the full set of data may be found in the supplementary information.

A first set of measurements was carried out to assess the optical loss of the whole structure: the laser at 1550 nm was coupled to each input and the power at the optical output port was optimised by opportune control of the MZIs (see supplementary information). The wavelength was then swept from 1500 nm to 1600 nm in order to analyse the wavelength dependence of the device. The results are reported in the graph of Fig. 4a, where the insertion loss (IL) is reported as a function of the input port and wavelength. The IL is maximal for 1500 nm, and minimal at 1600 nm with average values across the ports of 19.7 dB and 13.8 dB, respectively. At the typical optical communication wavelength, 1550 nm, the mean IL value is 15.7 dB with a standard deviation of 1.1 dB. Despite the considerable size of the chip, the majority

of the optical losses arise from the optical I/O and not from routing, as the former contributes around 5 dB/interface of loss and the latter introduces approximately ~ 0.1 dB/cm at 1550 nm. The remaining 5.7 dB of losses are introduced by the interferometers, of which there are 5 for each input-output path, resulting in an average IL of ~ 1.1 dB/MZI. The fact that losses decrease at higher wavelengths suggests that the MMIs are not at the correct working point at 1550 nm, likely as a result of a wider-than-designed central section.

A second set of measurements was carried out to evaluate the performance of the MZIs in terms of extinction ratio (ER), average power for a π shift in the thermal tuners (P_π), thermal crosstalk, and phase shifter bandwidth. Fig. 4b reports the interference fringes of MZI 1.1 as a function of applied bias voltage for its bar and cross port. 10 dBm of laser-light at 1550 nm was coupled individually to input 1 (cross) and input 2 (bar), and the consecutive MZIs were set to route all power to the output port. By sweeping the internal phase shifter voltage between 0 and 20 V, we evaluated an ER of 26.9 dB and 25.0 dB for the cross and bar states, respectively. The extinction ratio of all the MZIs in cross state was measured in a similar fashion, with an average value of 28.3 dB and a standard deviation of 2.4 dB. The performance of the MZIs is worse than expected by design: the IL should be lower, around 0.5 dB, and the ER should be around 40 dB. The π shift power was then derived by evaluating the bias voltage corresponding to the minimum and maximum transmission and considering the resistance of each phase shifter. The average P_π was measured to be 34.1 mW, with a standard deviation of 8.5 mW allowing for a total phase shift of more than 6π before failure. The P_π values in PICs usually have a low variance as they depend on the heater resistance, which in our case should have been 1 k Ω . Typically the P_π of similar phase shifters is close to 25 mW [25]. Here the excess and varying contact resistance of the heaters, with an average value of 4.1 k Ω and a standard deviation of 1.1 k Ω , and thus power dissipation, was due to

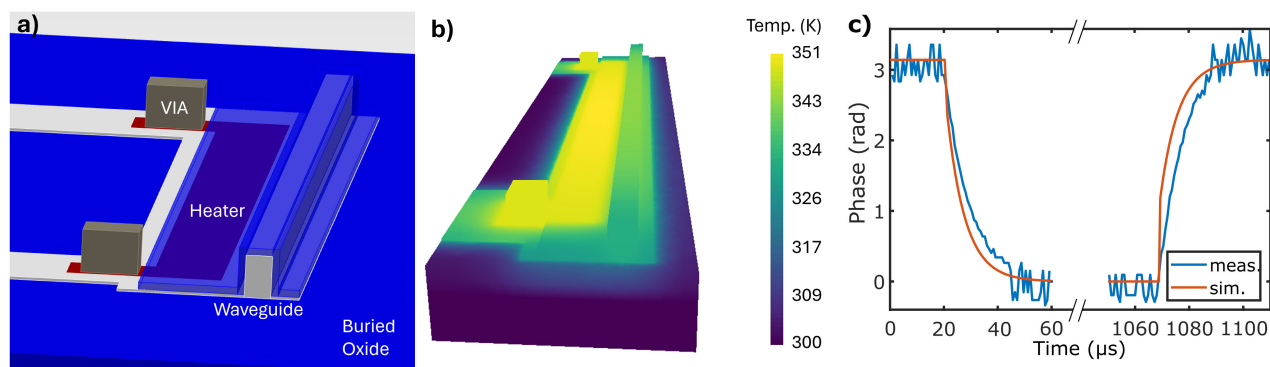


FIGURE 5. a) Lumerical HEAT and CHARGE simulation setup for the implanted heater response; b) thermal distribution in steady state when a V_{π} is applied to the shifter; c) comparison between the rise and fall signals for simulated and measured results.

the use of the contact metallization process optimized for the PDs. This single metal process was used for the whole chip, while optimized multi-metallization steps should be considered in the future. The list of all measured resistances can be found in the supplementary information.

The bandwidth of the phase shifters is limited by the delay between the time the voltage signal is applied and when thermal equilibrium is reached. To characterise this limit the phase shifters were driven with a square wave signal, with a frequency of around 1 kHz and peak to peak amplitude equal to V_{π} , the voltage required to change the phase by π , producing an optical signal that goes from maximum to minimum at the output port. Before the measurements, we derived the bandwidth of our DAC, which was >300 kHz. The setup for this measurement is depicted in the supplementary information. Before the fabrication of the circuit, the thermal phase shifters were numerically evaluated with Lumerical HEAT and CHARGE to predict the V_{π} step response time. Fig. 5a represents the simulation setup, composed of the thick-silicon slab waveguide, passivation silica, the electrical vias, a $100 \mu\text{m}$ thermal shifter that runs parallel to the waveguide, and below, a buried oxide layer. A conductive and thermal transient simulation was performed to evaluate the rise and fall times when V_{π} is applied to the electrical vias. Fig. 5b represents the thermal distribution at equilibrium when the heater is driven with V_{π} . The numerical analysis predicted a rise time of $7.81 \mu\text{s}$ (128 kHz) and a fall time of $9.03 \mu\text{s}$ (110 kHz). Fig. 5c compares the fall and rise signals, converted in relative phase shift, between the simulation and the experimental acquisition from the photodiode under actuation of the internal shifter of MZI 4.1.

Fig. 6a illustrates how the rise and fall times are calculated for MZI 4.1. The symbols, t_{ro} and t_{fo} , correspond to the optical rise and fall times respectively. Since the MZI is being driven in cross state, t_{fo} corresponds to when the phase shifter is heating (rise time) and t_{ro} when the phase shifter is not activated and the device is returning to room temperature (fall time). In this instance, $t_{ro} = 1.23 \times 10^{-5}$ s and $t_{fo} = 1.07 \times 10^{-5}$ s corresponding to respective limits in

bandwidth of 81 kHz and 94 kHz. Four phase shifters were characterised in this way, the mean values of rise and fall time were calculated over several modulation cycles, resulting to be $12.4 \mu\text{s}$ (80.6 kHz) and $9.4 \mu\text{s}$ (106 kHz), respectively.

Since the thermalisation time is dependent on the temperature of the PIC, for MZI 1.1, a characterization was performed in a range of temperatures from 10°C to 40°C , to simulate the operation of the PIC in different environmental conditions. Fig. 6b reports the results of this investigation, showing a notable increase in the fall time, as expected from the reduced temperature gradient, when the heater is switched off. These phase shifters are fast enough to use in a coherent combination context, for which a 50 kHz modulation at small amplitude (≤ 1 radians) was proposed [30]. The thermal cross talk effect between the internal shifter of MZI 1.1 and the surrounding phase shifters was investigated by coupling light into port 1, setting the voltage at the internal shifter such that the power at the output port was at a minima (more sensitive to changes in temperature), and measuring the output power for both 0 V and 20 V applied to the closest surrounding phase shifters (corresponding to $>2\pi$ phase change). The maximum observed change in output power resulting from the cross talk was 2.1 dB corresponding to a change in phase of 0.074 radians, when the external phase shifter of MZI 1.1 was heated, it was less than 0.3 dB (0.031 radians) for all other cases. The very low thermal crosstalk is ensured by the deep trenches around the heater and waveguides of the VTT Silicon process [25].

A final set of measurements was carried out to assess the germanium photodiode performance in terms of dark current, responsivity, and optical bandwidth. Without any optical input, the dark current was measured as a function of bias for three different photodiodes (1.7, 1.16, 2.3), the average values at 0 V, 1 V and 2 V of negative bias are 1.1 ± 0.3 nA, 764 ± 74 nA and 1096 ± 128 nA respectively. For photodiode 2.3, the dark current was also measured as a function of both bias and temperature with results reported in Table 1a, when negative bias was applied there was around four times as much dark current at a temperature of 40°C compared to

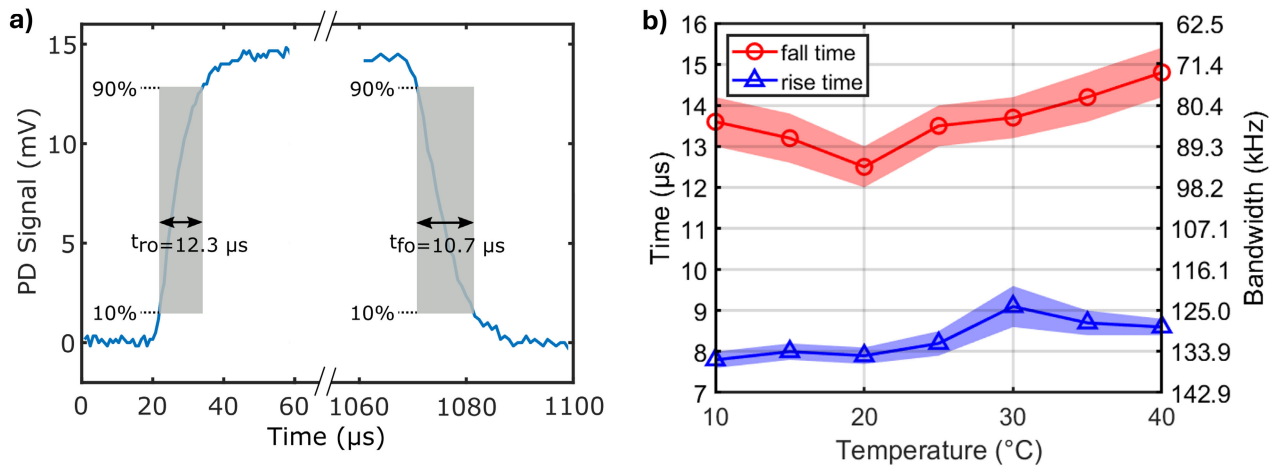


FIGURE 6. a) Signal at PIC output during phase shifter modulation to show how rise time, t_{fo} , and fall time, t_{ro} , are calculated. b) Rise time, fall time and associated limits in bandwidth of MZI 1.1 as a function of temperature with shaded region representing ± 1 standard deviation.

10 °C. The PD responsivity was estimated ≈ 0.8 A/W in DC by monitoring the output current when 10 dBm power of laser was injected, considering the coupling and propagation losses.

The measurement of the 3 dB bandwidth of the monitor PDs could not be performed using the packaged PIC, as these were wirebonded to DC connectors. The PDs were characterised on a naked chip fabricated in the same run and wafer at a probe station. The laser was coupled to an external modulator with >25 GHz bandwidth, whose output was divided by a 3-dB splitter with one branch leading to a 50 GHz PD with a known bandwidth response, and the other to a SMF fiber which was edge coupled to the optical inputs on the chip. A microwave vector network analyzer was used with the output port coupled to the modulator input port, one receiver port was connected to the known PD and the other to a RF probe used to contact the PDs on the chip. This setup is represented in the supplementary information. Different negative biases were supplied with a bias-tee at the RF probe, with the DC port connected to a source measure unit. With this configuration we subtracted the response of the known PD branch from the S_{21} response of the device under test, to compensate for the response of the RF equipment common to both outputs. The S_{21} frequency response of the known PD itself and the RF tip were then removed, and with a separate characterization, a correction was applied for the difference in output signal paths (only one had a bias-tee). With this method, the 3 dB bandwidths at differing negative bias were characterised for 4 photodiodes selected in different areas of the PIC; Table 1b reports these results. An example of a typical PD response, in this case for PD 2.1, as a function of applied negative bias is shown in Fig. 7, where the dashed horizontal line corresponds to -3 dB. The germanium photodetectors showed a large bandwidth increase by applying the first 0.5 V of negative bias, (from 2.6 to 7.5 GHz for PD 2.1), with a less pronounced

improvement as the negative bias was increased. As the monitor photodiodes for the adaptive optics algorithm read signals at some tens of kHz, zero bias may be used as it provides sufficient bandwidth and a very low dark current (on the order of few nA), that would otherwise increase significantly.

IV. DISCUSSION

The device thermal phase shifters surpassed the target bandwidth of 50 kHz, while providing a sufficient number of π shifts ($> 6\pi$) to be used with an appropriate control algorithm in real time. The measured low thermal crosstalk and consistent ER of the MZIs ensure the correct functionality when coherently recombining 32 input lightwaves. The power consumption of our device is < 4.5 mW, considering an average of 2π per heater. This is considerably lower in respect to classical adaptive optics solutions based on deformable mirrors, where the power consumption spans from tens to hundreds of Watts [31], [32].

The main shortcoming which prevents the use of the presented coherent combiner in realistic applications resides in the losses, which resulted much higher than expected, as discussed in the previous section. The main contribution resides in the optical I/O, accounting for 5 dB per facet, with the MZIs also contributing, whose constituent MMI were fabricated wider than designed, leading to an overall average loss of 15.7 dB at 1550 nm. However, the losses can be considerably reduced in future fabrications through the addition of the optical interposer chip inserted between the SMFs and the PIC, which lowers the coupling losses to 1.5 dB per facet. Moreover, the current VTT process has waveguides with improved smoothness thanks to a hydrogen-annealing step, thus reducing the propagation losses with a demonstrated value of just 0.027 dB/cm, a more than threefold improvement with respect to the previous value of 0.1 dB/cm [33]. Finally, the IL of each MZI can be

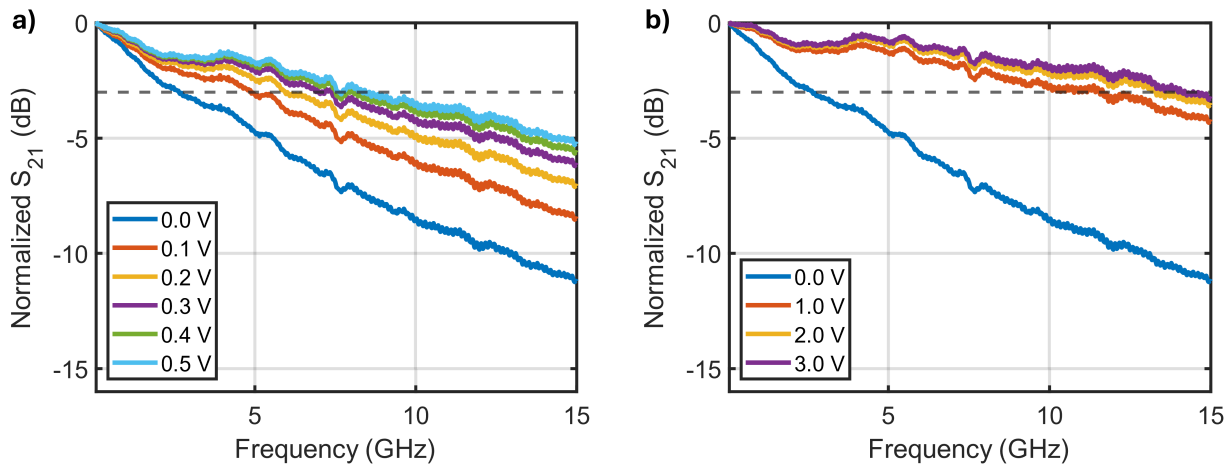
TABLE 1. a) Dark currents for photodiode 2.3 as a function of bias and temperature and bias. b) 3 dB bandwidth for different photodiodes as a function of bias.

Temp (°C)	Dark Current (nA)		
	0V	-1V	-2V
10	1.9	496.4	714.1
15	1.6	633.4	906.0
20	1.5	791.8	1125.5
25	1.6	1004.6	1426.0
30	1.5	1258.3	1788.2
35	1.7	1553.0	2236.1
40	1.7	1932.2	2794.7

(a)

PD	Bandwidth (GHz)				
	0.0V	-0.5V	-1.0V	-1.5V	-2.0V
1.1	2.6	9.1	11.8	13.3	14.1
2.1	2.6	7.5	10.2	11.8	13.2
4.2	4.4	8.6	11.8	13.3	14.2
1.16	2.1	7.5	11.8	13.6	15.0

(b)

**FIGURE 7.** Normalized S_{21} response of photodiode 2.1 for a range in reverse bias a) 0.0 V - 0.5 V b) 0.0 V - 3.0 V. The horizontal grey dashed line corresponds to -3 dB.

lowered to ≤ 0.5 dB/MZI with a correct fabrication of the constituent MMIs [25]. With this performance, the same chip with 32 inputs would have a total loss of 5.5 dB, accounting for 2 optical I/O and 5 MZI encountered by each path, and disregarding propagation losses. In the case of a 64-input device, the losses increase by 0.5 dB as there is one additional MZI in all input-output paths.

Aside from improvements in the losses, the PIC power consumption can be decreased considerably: the thermal phase shifter contact resistance should be lower, granting a $P_{\pi} \leq 25$ mW, instead of the 34.1 mW found with the current chip. Moreover, the heater thermal isolation can be further improved by removing the silicon substrate underneath the heater, leading to a P_{π} on the order of 1 mW [25]. Table 2 reports a comparison between our work and other coherent combiner PICs from the literature. In the last column, we have reported the prospective performance of a 32/64-input coherent combiner according to the latest demonstrated performance of the VTT process and introduction of an interposer, as discussed above. The table reports number of supported modes (inputs), footprint, whether the PIC has integrated PDs, average total loss, phase shifter rise/fall time, P_{π} , and MZI IL. Although our chip has the highest optical losses at telecom wavelength, it demonstrated good performance in terms of MZI IL, phase shifter rise/fall

time, and power consumption. Our chip achieves a small footprint, which translates directly into low manufacturing costs. The only other works that reports the footprint are that of Billaud et al. [19] and Martinez et al. [20], with a value of 1 cm^2 for an 8-input device and 0.04 cm^2 for a 16 input device, compared to the 0.5 cm^2 of our device with 32-inputs. Nonetheless, a smaller footprint is ensured in principle when using VTT Thick SOI instead of standard 220 nm SOI [25], hence the footprint can be optimally minimized in perspective devices. The confinement of the light mode to the $3 \mu\text{m}$ waveguide, combined with the deep trenches, give our chip unique thermal isolation and stability features, making it possible to use all 62 thermal phase shifters without the need for electrical stabilization control loops. As discussed by L. Rinaldi [34], a 32-input chip is suitable for medium-small turbulence, typical of horizontal links and LEO satellites close to the zenith. Thus, our chip is the only one that allows mitigation in these condition, with the exception of that of Billaud [23]. However, the latter chip has no integrated photodiodes, which increases the system size and the complexity of the surrounding electronics: 44 bulk photodiodes are required along with the corresponding electronics. The combination of low propagation losses, low footprint, and excellent thermal isolation allows our chip to be effectively scaled towards a

TABLE 2. Comparison between the fabricated unitary optical processors and other MZI-based reconfigurable chips. GC: Grating Coupler; SSC: Spot Size Converter; EC: Edge Coupler.

PIC Combiner	Billaud [19]	Billault [18]	Martinez [20]	Billaud [23]	This work	Prospective
# inputs	8	15	16	45	32	32 / 64
Platform	SOI	SOI	SOI	SOI	Thick SOI	Thick SOI
Footprint (cm ²)	≈ 1	NA	0.04	NA	0.5	0.5 / 1.0
Integrated PDs	Yes	Yes	Yes	No	Yes	Yes
Avg losses (dB)	9.8	7-11	13.6	9	15.7	5.5 / 6.0
Rise time (μs)	10	≈ 25	NA	5.1	12.4	≈ 10
Fall time (μs)	7.6	≈ 25	NA	NA	9.4	≈ 10
P _π (mW)	<40	NA	≈ 20	NA	34.1	≤ 25
MZI IL (dB)	≈ 1	0.6	NA	NA	1.1	≤ 0.5

higher number of inputs. A prospective device would have the lowest losses even with a 64 input configuration, while also improving the power consumption. A 64-input device would also allow the mitigation of strong turbulence conditions, such as those encountered for LEO satellites close to the horizon.

To further reduce the losses, the combiner architecture can be changed to enable phase-only correction of the decomposed modes [30]. This can be easily done by substituting the MZIs in the binary tree architecture with 3-dB (50/50) 2×2 directional couplers, or equivalently MMIs. Here, the phase control is implemented by two thermal tuners at the inputs of each element, while the feedback for the control loop is collected by a PD at an output of each coupler. For the VTT process, the MMI IL is ≤ 0.2 dB instead of the ≈ 0.5 dB for an MZI [25], so accounting for 1.5 dB per I/O interface, a 32-input combiner would have an overall loss of 4 dB, and a 64-input combiner would have 4.2 dB of loss, where propagation losses are neglected as extremely low (0.027 dB/cm with hydrogen-annealing). However, a phase-only correction of the input modes is equivalent to the MZI scheme only if the modes have the same amplitude. In a realistic scenario, the amplitudes can be modeled as independent random variables following a Rayleigh distribution. For this reason, as discussed by L. Rinaldi [34], in a phase-only device a higher number of modes is required for an equivalent correction: around 25 for medium-small turbulence, and more than a hundred for strong turbulence. These numbers can be reduced to 16 and 64 respectively, if a tip-tilt correction is implemented in the receiving chain before mode decomposition [34].

V. CONCLUSION AND FUTURE WORK

Free space optical links enable wireless communication at high data rates, and are envisaged as a key component of future communication systems, spanning 5G/6G, quantum links, and satellite communications. However, atmospheric turbulence introduces distortions to the beam which limits the effective use of FSO in horizontal and satellite links.

Here, we have reported the design, fabrication, and characterization of an integrated coherent optical combiner for turbulence mitigation in free space optical links. The PIC was fabricated with the Thick SOI open platform offered by VTT, featuring 32 inputs and containing 31 integrated MZIs and photodetectors. The phase shifters were found to have a bandwidth of 81 kHz, an average P_π of 34.1 mW, and are able to shift the phase by more than 6π , meeting the requirements for turbulence correction in horizontal and LEO-to-ground links. Due to fabrication problems, the chip losses were much higher than expected, with an average value of 15.7 dB at a wavelength of 1550 nm. This is the main shortcoming preventing its use in real scenarios.

Nonetheless, by leveraging an optical interposer and the reduced losses offered by the new VTT process, a prospective device with the same number of inputs would reduce the losses to just 5.5 dB. For a 64 input device, the losses would increase to 6 dB, lower than any fabricated PIC combiner in literature. These numbers can be further reduced to 4 dB and 4.2 dB respectively if the device were to implement a phase-only correction.

Our future work will be to design improved versions of this chip, both with phase-only and amplitude-phase correction abilities. Particular effort will be put in the further reduction of I/O losses with edge coupling. At the present state, using the optical interposer would decrease the coupling losses to ≤ 1.5 dB/facet [25]. Reaching 0.8 dB/facet would allow future chips to be used in a complete FSO receiver. As a next step, we plan to use the presented chip in an experimental demonstration of horizontal and LEO satellite-to-ground FSO communication links, to test its effectiveness in implementing turbulence mitigation.

ACKNOWLEDGMENT

The authors would like to thank Dr. L. Rinaldi for fruitful discussions about his work on atmospheric turbulence mitigation. They also acknowledge several of VTT's experts in Si photonics fabrication and PIC packaging for implementing the prototype device.

REFERENCES

- [1] J. Poliak, R. M. Calvo, and F. Rein, "Demonstration of 1.72 Tbit/s optical data transmission under worst-case turbulence conditions for ground-to-geostationary satellite communications," *IEEE Commun. Lett.*, vol. 22, no. 9, pp. 1818–1821, Sep. 2018.
- [2] S. A. Al-Gailani, M. F. M. Salleh, A. A. Salem, R. Q. Shaddad, U. U. Sheikh, N. A. Algeelani, and T. A. Almohamad, "A survey of free space optics (FSO) communication systems, links, and networks," *IEEE Access*, vol. 9, pp. 7353–7373, 2021.
- [3] S. Dang, O. Amin, B. Shihada, and M.-S. Alouini, "What should 6G be?" *Nature Electron.*, vol. 3, no. 1, pp. 20–29, Jan. 2020.
- [4] M. Toyoshima, "Recent trends in space laser communications for small satellites and constellations," *J. Lightw. Technol.*, vol. 39, no. 3, pp. 693–699, Feb. 1, 2021.
- [5] S.-K. Liao et al., "Satellite-to-ground quantum key distribution," *Nature*, vol. 549, no. 7670, pp. 43–47, 2017.
- [6] E. Fischer, M. Feriencik, K. Kudielka, T. Dreischer, P. Adolph, T. Berkefeld, D. Soltau, J. Perdigues-Armengol, and Z. Sodnik, "ESA optical ground station upgrade with adaptive optics for high data rate satellite-to-ground links-test results," in *Proc. IEEE Int. Conf. Space Opt. Syst. Appl. (ICSOS)*, Oct. 2019, pp. 1–6.
- [7] D. Kolev, K. Shiratama, A. Carrasco-Casado, Y. Saito, Y. Munemasa, J. Nakazono, P. V. Trinh, H. Kotake, H. Kunimori, T. Kubooka, T. Fuse, and M. Toyoshima, "Status update on laser communication activities in NICT," in *Proc. IEEE Int. Conf. Space Opt. Syst. Appl. (ICSOS)*, Kyoto City, Japan, Mar. 2022, pp. 36–39.
- [8] L. C. Roberts, S. R. Meeker, J. Tesch, J. C. Shelton, J. E. Roberts, S. F. Fregoso, T. Troung, M. Peng, K. Matthews, H. Herzog, and J. Rodriguez, "Performance of the adaptive optics system for laser communications relay demonstration's ground station 1," *Appl. Opt.*, vol. 62, no. 23, p. 26, Aug. 2023.
- [9] C. Petit, A. M. Bonnefois, E. Chalali, F. Gustave, K. Caillaud, L. Krafft, Y. Lai-Tim, J. Montri, L. Paillier, P. Perrault, J.-B. Volatier, D. B. Dubosc, and N. Védrenne, "Onera's optical ground station for geo feeder links FEELINGS: In lab testing and on sky implementation," in *Proc. IEEE Int. Conf. Space Opt. Syst. Appl. (ICSOS)*, Vancouver, BC, Canada, Oct. 2023, pp. 193–197.
- [10] L. B. Stotts, B. Stadler, D. H. Hughes, P. Kolodzy, A. Pike, D. W. Young, J. E. Sluz, J. C. Juarez, B. Graves, D. Dougherty, J. Douglass, and T. Martin, "Optical communications in atmospheric turbulence," *Proc. SPIE*, vol. 7464, pp. 21–37, Aug. 2009.
- [11] M. Li, W. Gao, and M. Cvijetic, "Slant-path coherent free space optical communications over the maritime and terrestrial atmospheres with the use of adaptive optics for beam wavefront correction," *Appl. Opt.*, vol. 56, no. 2, pp. 284–297, Jan. 2017.
- [12] E. Ciaramella, Y. Arimoto, G. Contestabile, M. Presi, A. D'Errico, V. Guarino, and M. Matsumoto, "1.28 terabit/s (32×40 Gbit/s) WDM transmission system for free space optical communications," *IEEE J. Sel. Areas Commun.*, vol. 27, no. 9, pp. 1639–1645, Dec. 2009.
- [13] C. A. Primmerman, T. R. Price, R. A. Humphreys, B. G. Zollars, H. T. Barclay, and J. Herrmann, "Atmospheric-compensation experiments in strong-scintillation conditions," *Appl. Opt.*, vol. 34, no. 12, pp. 2081–2088, Apr. 1995.
- [14] N. Schwartz, "Précompensation des effets de la turbulence par optique adaptative: Application aux liaisons optiques en espace libre," Ph.D. thesis, Dept. Phys., Université Nice Sophia Antipolis, 2009.
- [15] T. R. O'Meara, "The multidither principle in adaptive optics," *J. Opt. Soc. Amer.*, vol. 67, no. 3, pp. 306–315, Mar. 1977.
- [16] T. M. Shay, V. Benham, J. T. Baker, B. Ward, A. D. Sanchez, M. A. Culpepper, D. Pilkington, J. Spring, D. J. Nelson, and C. A. Lu, "First experimental demonstration of self-synchronous phase locking of an optical array," *Opt. Exp.*, vol. 14, no. 25, pp. 12015–12021, Dec. 2006.
- [17] Y. Ma, P. Zhou, X. Wang, H. Ma, X. Xu, L. Si, Z. Liu, and Y. Zhao, "Coherent beam combination with single frequency dithering technique," *Opt. Lett.*, vol. 35, no. 9, pp. 1308–1310, May 2010.
- [18] V. Billault, J. Bourderionnet, J. P. Mazellier, L. Leviandier, P. Feneyrou, A. Maho, M. Sotom, X. Normandin, H. Lonjaret, and A. Brignon, "Free space optical communication receiver based on a spatial demultiplexer and a photonic integrated coherent combining circuit," *Opt. Exp.*, vol. 29, no. 21, pp. 33134–33143, 2021.
- [19] A. Billaud, A. Reeves, A. Orioux, H. Frief, F. Gomez, S. Bernard, T. Michel, D. Allieux, J. Poliak, R. M. Calvo, and O. Pinel, "Turbulence mitigation via multi-plane light conversion and coherent optical combination on a 200 m and a 10 km link," in *Proc. IEEE Int. Conf. Space Opt. Syst. Appl. (ICSOS)*, Mar. 2022, pp. 85–92.
- [20] A. I. Martinez, G. Cavicchioli, S. Seyedinavadeh, F. Zanetto, M. Sampietro, A. D'Acerno, F. Morichetti, and A. Melloni, "Self-adaptive integrated photonic receiver for turbulence compensation in free space optical links," *Sci. Rep.*, vol. 14, no. 1, p. 20178, Aug. 2024.
- [21] N. Védrenne, J.-M. Conan, C. Petit, and V. Michau, "Adaptive optics for high data rate satellite to ground laser link," *Proc. SPIE*, vol. 9739, pp. 119–128, Mar. 2016.
- [22] T. Michel, A. Orioux, C. Dautancourt, T. Luttmann, S. Bernard, C. Autebert, L. Andréoli, P. Jian, D. Allieux, O. Pinel, G. Labroille, and A. Billaud, "100 Gbps and 45-mode multi-plane-light-conversion-based turbulence mitigation for free space optical communication," *Proc. SPIE*, vol. 12413, Mar. 2023, Art. no. 1241310.
- [23] A. Billaud, C. Dautancourt, T. Luttmann, C. Autebert, T. Michel, P. Jian, O. Pinel, and G. Labroille, "TILBA-ATMO: A 45-mode MPLC-based turbulence mitigation solution for optical ground stations for direct-to-Earth LEO-to-ground laser communications," *Proc. SPIE*, vol. 12877, Mar. 2024, Art. no. 128771D.
- [24] P. S. Kincaid, L. De Marinis, G. Contestabile, V. Michau, Y. Lucas, L. Krafft, M. Karppinen, and M. Cherchi, "A 32-input integrated coherent combiner," in *Proc. IEEE Photon. Soc. Summer Topicals Meeting Ser. (SUM)*, Jul. 2024, pp. 1–2.
- [25] T. Aalto, M. Cherchi, M. Harjanne, S. Bhat, P. Heimala, F. Sun, M. Kapulainen, T. Hassinen, and T. Vehmas, "Open-access 3- μm SOI waveguide platform for dense photonic integrated circuits," *IEEE J. Sel. Topics Quantum Electron.*, vol. 25, no. 5, pp. 1–9, Sep. 2019.
- [26] D. W. Young, H. H. Hurt, J. E. Sluz, and J. C. Juarez, "Development and demonstration of laser communications systems," *Johns Hopkins APL Tech. Dig.*, vol. 33, no. 2, pp. 122–136, 2015.
- [27] L. De Marinis, N. Andrioli, and G. Contestabile, "Analysis of integration technologies for high-speed analog neuromorphic photonics," *IEEE J. Sel. Topics Quantum Electron.*, vol. 29, no. 6, pp. 1–9, Nov./Dec. 2023.
- [28] S. Y. Siew, B. Li, F. Gao, H. Y. Zheng, W. Zhang, P. Guo, S. W. Xie, A. Song, B. Dong, L. W. Luo, C. Li, X. Luo, and G.-Q. Lo, "Review of silicon photonics technology and platform development," *J. Lightw. Technol.*, vol. 39, no. 13, pp. 4374–4389, Jul. 1, 2021.
- [29] D. A. B. Miller, "Self-aligning universal beam coupler," *Opt. Exp.*, vol. 21, no. 5, pp. 6360–6370, Mar. 2013.
- [30] Y. Lucas, V. Michau, and S. Meimon, "Spatial diversity control law for demultiplexer and active photonic integrated circuits for atmospheric effect mitigation," *Proc. SPIE*, vol. 12877, pp. 220–236, Mar. 2024.
- [31] *Alpao Deformable Mirrors*. Accessed: Jan. 11, 2025. [Online]. Available: <https://www.alpao.com/products-and-services/deformable-mirrors/>
- [32] *Thorlabs Deformable Mirrors*. Accessed: Jan. 11, 2025. [Online]. Available: https://www.thorlabs.com/NewGroupPage9_PF.cfm?Guide=10&Category_ID=220&ObjectGroup_ID=5056
- [33] Y. E. Marin, A. Bera, M. Cherchi, and T. Aalto, "Ultra-high-Q racetrack resonators on thick SOI platform through hydrogen annealing smoothing," *J. Lightw. Technol.*, vol. 41, no. 11, pp. 3642–3648, Jun. 1, 2023.
- [34] L. Rinaldi, "Mitigation of atmospheric turbulence effects on optical links by integrated optics," Doctoral thesis, Dept. Phys., Université de Paris Saclay, 2022.

LORENZO DE MARINIS (Member, IEEE) received the B.S. and M.S. degrees in electronic engineering from the University of Pisa, in 2017 and 2019, respectively, and the Ph.D. degree from Scuola Superiore Sant'Anna (SSSA), Pisa, Italy, in 2022. From November 2021 to April 2022, he was a Visiting Scholar at the WinPhoS Laboratory, Aristotle University of Thessaloniki, Thessaloniki, Greece. From September 2022 to February 2023, he was a Research Fellow in quantum and neuromorphic photonics at SSSA, where he is currently an Assistant Professor. His main research interests include the conceptualization and design of photonic integrated circuits for quantum and neuromorphic applications, analog computing, photonic-electronic co-design, and machine learning for networking scenarios.

PETER SEIGO KINCAID (Member, IEEE) received the M.Sc. degree in physics (international study) from the University of Birmingham, in 2018, and the Ph.D. degree in applied physics from the University of Pisa, in 2023. He is currently an Assistant Professor at Scuola Superiore Sant'Anna, Pisa, and a Marie Curie Fellow with the University of Pisa. His research interests include photonic neuromorphic computing, integrated photonics, free space optics communications, and quantum random number generation.

YANN LUCAS received the Engineering and M.S. degrees in physics and photonics from Télécom Physique Strasbourg, France, specializing in photonics for nanosciences and life sciences, and the Ph.D. degree from Paris-Saclay University, in 2024, with a focus on integrated adaptive optics for atmospheric turbulence effects mitigation on optical links. In 2025, he joined the Department of Optics, ONERA.

LEA KRAFFT received the Engineering and M.S. degrees in physics and photonics from Télécom Physique Strasbourg, France, specializing in photonics for nanosciences and life sciences, and the Ph.D. degree from Paris-Saclay University, in 2022, with a focus on adaptive optics retinal imaging and the study of scattering in complex media. In 2023, she joined the Department of Optics, ONERA. Her current research interests include aberration mitigation and the development of imaging systems, focusing on light propagation and deep imaging applications in tissues, atmospheric, and underwater environments.

VINCENT MICHAU received the Ph.D. degree in physics, in 1989. Since 1988, he has been with ONERA, where he developed wave-front sensors, adaptive optics systems, and turbulence monitoring devices. He has been the project manager of several projects in high angular resolution imaging, the Head of the High Angular Resolution Research Unit, and a Scientific Assistant with the Department of Optics, ONERA. Today, he is particularly interested in the application of photonic circuits to imaging and correction of the effects of atmospheric turbulence on laser beams. He is the author or co-author of more than 180 publications in journals or conferences.

MATTEO CHERCHI received the first M.Sc. degree in physics from the University of Pavia, Italy, the second M.Sc. degree in applied mathematics from the University of Cambridge, U.K., and the Ph.D. degree from the Department of Electronics Engineering, University of Palermo, Italy. After some years, he spent basic research in the industry (former Pirelli Labs-Optical Innovation). He has been a Postdoctoral Research Associate with the Group of Prof. Michael R. Watts (RLE at MIT) and then joined the Silicon Photonics Group, VTT Technical Research Centre of Finland. He is currently a Principal Photonics Engineer at Xanadu Quantum Technologies. He has 25 years of experience in integrated optics, both in industrial research and academia.

MIKKO KARPPINEN received the M.Sc. degree in engineering physics from Aalto University, Espoo, Finland, and the D.Sc. degree in optoelectronics from the University of Oulu, Oulu, Finland. Since 1998, he has been working on photonics device integration, fabrication, and packing with the VTT Technical Research Centre of Finland. He is currently leading the team on photonics and RF integration.

GIAMPIERO CONTESTABILE received the Laurea degree in physics from the Sapienza University of Rome, Rome, Italy, in 1998, and the Ph.D. degree in electrical engineering and telecommunications from the University of Rome "Tor Vergata," in 2001. From 1996 to 2000, he was with the Semiconductor Devices Group, Fondazione Ugo Bordoni, Rome. In 2001, he was with Opto Speed Italia. He is currently an Associate Professor with Scuola Superiore Sant'Anna, Pisa, Italy. He has co-authored more than 200 papers published in international peer-reviewed journals and presented at leading international conferences. His research interests include photonic integrated circuits, advanced optical systems, access networks, and semiconductor optical amplifiers and lasers.

• • •